

# Improving resolution by means of ghost imaging

Pengli Zhang, Wenlin Gong, Xia Shen, Dajie Huang and Shensheng Han\*  
 Key Laboratory for Quantum Optics and Center for Cold Atom Physics,  
 Shanghai Institute of Optics and Fine Mechanics,  
 Chinese Academy of Sciences, Shanghai 201800, China  
 (Dated: November 24, 2018)

As one of important analysis tools, microscopes with high spatial resolution are indispensable for scientific research and medical diagnosis, and much attention is always focused on the improvement of resolution. Over the past decade, a novel technique called ghost imaging has been developed that may provide a new approach toward increasing the resolution of an imaging system. In this paper, we introduce this technique into microscopes for the first time and report a proof-of-principle experimental demonstration of a microscope scheme based on ghost imaging.

PACS numbers: 42.30.Va, 42.50.Xa, 42.50.Ar, 68.37.Yz

During the past half century some sophisticated optical technologies, such as confocal microscopes [1, 2], transmission x-ray microscopes [3, 4] and so on, have been exploited to achieve excellent resolution. For a lens-based optical microscope, the resolution is determined by the extent of the point spread function, and the extent primarily depends on the wavelength of illumination light and the numerical aperture (NA) of the objective lens [5]. A lens with high NA is one of the key factors of realizing high resolution. However, some practical conditions may restrict the use of a high-NA lens. For example, medical endoscopes [6] examining human internal organs require lenses with small aperture and transmission x-ray microscopes [7] detecting thick specimens demand Fresnel zone plates with long focal depth, which both limit NAs of the lenses. The development [8, 9, 10, 11, 12, 13, 14, 15, 16, 17, 18, 19] of ghost imaging in recent ten years, now brings a new way to increase the resolution of these lens-limited microscopes.

Ghost imaging is a technique that forms an image of an object by measuring two correlated optical fields with the use of entangled sources [8] or “classical” sources, such as pairs of momentum-correlated laser pulses [9] and thermal light [12, 13]. In general, a conventional imaging system only needs one detector to record the intensity distribution related to the amplitude and phase of a target object. In quantum theory of photodetection, the light intensity measured by the detector can be represented by the first order correlation function [20]:

$$G^{(1)}(x, t) = \langle E^{(-)}(x, t)E^{(+)}(x, t) \rangle, \quad (1)$$

where  $E^{(\pm)}(x, t)$  are the quantized positive and negative frequency parts of the field at space-time location  $(x, t)$ . While a ghost imaging system must simultaneously record the intensities of two correlated beams: a beam that travels a path (the test arm) including the object and the other beam that passes through a reference optical system (the reference arm), the information about

the object is exacted from the correlation between two recorded intensities. The correlation can be evaluated through the second order correlation function [20]:

$$G^{(2)}(x_1, x_2, t, t) = \langle E^{(-)}(x_1, t)E^{(-)}(x_2, t)E^{(+)}(x_1, t)E^{(+)}(x_2, t) \rangle \quad (2)$$

where  $E^{(\pm)}(x_1, t)$  and  $E^{(\pm)}(x_2, t)$  are the field operators in two detecting planes at the same time. The unique work principle of ghost imaging leads to some interesting optical phenomena, such as reconstructing a “ghost” image in the reference arm while the measured object is in the test arm [8, 9, 12, 13], implementing coherent and incoherent imaging in the same system only by changing the detection modes [11], and lensless Fourier-transform imaging with thermal light [10], that the conventional imaging system can’t realize.

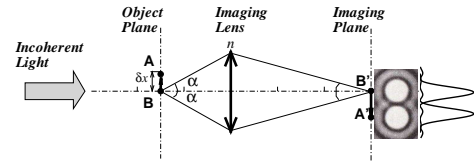


FIG. 1: Schematic of a simple conventional imaging system.  $n$  is refractive index of the medium, and  $\alpha$  is the half angle of the cone of light acceptable by the imaging lens.

A schematic of a simple conventional imaging system is shown in Fig.1. Under incoherent illumination, the image of a point at the object is not infinitely small, but is a circular diffraction image, or called diffraction spot. The width of the spot represents the resolution of the image. According to the Rayleigh criterion [21], the resolution limit of the system in the object plane is determined by

$$\delta x = 0.61 \frac{\lambda}{n \sin(\alpha)} \quad (3)$$

where  $n \sin(\alpha)$  denotes the NA of the imaging lens and  $\lambda$  is the wavelength of light. Eq.(3) shows that the improvement of resolution relies on shorter wavelength and

\*Electronic address: sshan@mail.shcnc.ac.cn

higher NA. While the wavelength is given and the lens is limited, it's still desirable to obtain high-resolution images. To achieve this goal, we apply ghost imaging technique into the conventional imaging system and present the theoretical and experimental demonstration of a new microscope scheme.

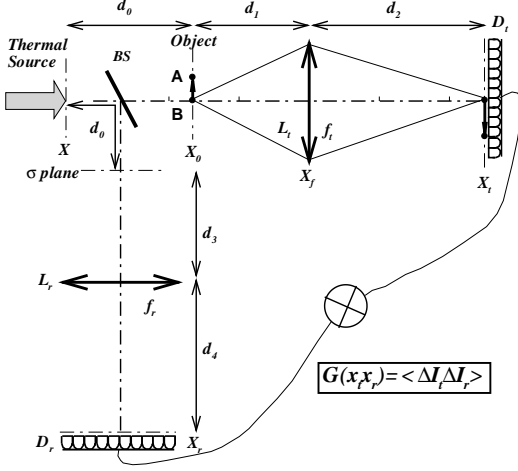


FIG. 2: The experimental setup of a two-arm imaging system based on ghost imaging.  $d_0$  is the distance from the light source to an object as well as to the  $\sigma$  plane. A lens with focal length  $f_t$  and aperture  $L_t$  is inserted in the test arm (including the object), and a lens with focal length  $f_r$  and aperture  $L_r$  in the reference arm. Both arms are two independent image-forming systems.  $d_1$ ,  $d_2$ ,  $d_3$  and  $d_4$  satisfy the Gaussian thin-lens equation:  $1/d_1 + 1/d_2 = 1/f_t$  and  $1/d_3 + 1/d_4 = 1/f_r$ .

On the base of Fig.1, we add another optical path and rebuild it into a new two-arm imaging system based on ghost imaging [see Fig.2], and here we just consider the case of thermal light illumination. A beam splitter (BS) behind the thermal source divides light into two beams propagating through two distinct arms: in the test arm, a lens with focal length  $f_t$  is placed distance  $d_1$  from an object and  $d_2$  from a detector  $D_t$ ; in the reference arm, for simplicity assuming a pseudo plane ( $\sigma$  plane) at the symmetric position of the object with respect to BS, a lens with focal length  $f_r$  is placed distance  $d_3$  from the  $\sigma$  plane and  $d_4$  from another detector  $D_r$ . The relevant distances obey the Gaussian thin-lens equation:  $1/d_1 + 1/d_2 = 1/f_t$  and  $1/d_3 + 1/d_4 = 1/f_r$ , which indicates

both arms are two independent image-forming systems, and are imaging the object and the  $\sigma$  plane, respectively. Although the image of the object can be obtained by the test arm directly, we pay more attention to the image reconstructed through the correlation between the two arms. Recording the test arm intensity  $I_t(x_t)$  by  $D_t$ , and correlating it with the reference arm intensity  $I_r(x_r)$  recorded by  $D_r$ , we can gain information about the object from the correlation function [11]

$$G(x_t, x_r) = \langle I_t(x_t) I_r(x_r) \rangle - \langle I_t(x_t) \rangle \langle I_r(x_r) \rangle. \quad (4)$$

In term of results of Ref.[10, 11, 15], Eq.(4) can be written as

$$G(x_t, x_r) = \left| \int_{source} dx dx' G^{(1)}(x, x') h_t(x, x_t) h_r^*(x', x_r) \right|^2, \quad (5)$$

where  $G^{(1)}(x, x')$  is the first order correlation function of the source, and  $h_t, h_r$  are the impulse response functions of the test arm and the reference arm, respectively. Suppose the source is quasimonochromatic and fully spatially incoherent:

$$G^{(1)}(x, x') = I(x) \delta(x - x') \quad (6)$$

where  $I(x)$  represents the intensity distribution of the source and  $\delta(x)$  is the Dirac delta function. Substituting Eq.(6) into Eq.(5), we have

$$G(x_t, x_r) = \left| \int_{source} dx I(x) h_t(x, x_t) h_r^*(x, x_r) \right|^2. \quad (7)$$

Further, under the paraxial approximation, the impulse response function of the test arm is given by

$$h_t(x, x_t) = \int dx_0 h_1(x, x_0) t(x_0) h_2(x_0, x_t), \quad (8)$$

where  $t(x_0)$  denotes the object transmission function,

$$h_1(x, x_0) = \frac{e^{jk d_0}}{j \lambda d_0} \exp \left\{ \frac{i \pi (x - x_0)^2}{\lambda d_0} \right\} \quad (9)$$

represents free-space propagation from the source to the object, and

$$h_2(x_0, x_t) = \int_{-\frac{L_t}{2}}^{\frac{L_t}{2}} dx_f \frac{e^{jk d_1}}{j \lambda d_1} \exp \left\{ \frac{i \pi (x_0 - x_f)^2}{\lambda d_1} \right\} \exp \left( -\frac{i \pi x_f^2}{\lambda f} \right) \frac{e^{jk d_2}}{j \lambda d_2} \exp \left\{ \frac{i \pi (x_t - x_f)^2}{\lambda d_2} \right\} \propto \text{sinc} \left\{ \left( \frac{x_0}{d_1} + \frac{x_t}{d_2} \right) \frac{L_t}{\lambda} \right\} \quad (10)$$

describes the one-dimensional (1-D) amplitude point spread function (APSF) of the lens of the test arm.  $\lambda$  is the source wavelength,  $k = 2\pi/\lambda$  is wave number, and  $L_t$  is the aperture of the lens in the test arm. Substituting Eq.(9)-Eq.(10) into Eq.(8), we get

$$h_t(x, x_t) \propto \int dx_0 \frac{e^{jk d_0}}{j \lambda d_0} \exp \left\{ \frac{i \pi (x - x_0)^2}{\lambda d_0} \right\} t(x_0) \text{sinc} \left\{ \left( \frac{x_0}{d_1} + \frac{x_t}{d_2} \right) \frac{L_t}{\lambda} \right\}. \quad (11)$$

Similarly to  $h_t(x, x_t)$ , the impulse response function of the reference arm is directly given by

$$h_r(x, x_r) \propto \int dx'_0 \frac{e^{jk d_0}}{j \lambda d_0} \exp \left\{ \frac{i \pi (x - x'_0)^2}{\lambda d_0} \right\} \text{sinc} \left\{ \left( \frac{x'_0}{d_3} + \frac{x_r}{d_4} \right) \frac{L_r}{\lambda} \right\}. \quad (12)$$

where  $L_r$  is the aperture of the lens in the reference arm. If the source is infinitely large and the intensity distribution is uniform,  $I(x) = I_0$ ; then substituting Eq.(11)-Eq.(12) into Eq.(7), after calculation, we obtain

$$\begin{aligned} G(x_t, x_r) &\propto I_0^2 \left| \int dx_0 t(x_0) \text{sinc} \left\{ \left( \frac{x_0}{d_1} + \frac{x_t}{d_2} \right) \frac{L_t}{\lambda} \right\} \text{sinc} \left\{ \left( \frac{x_0}{d_3} + \frac{x_r}{d_4} \right) \frac{L_r}{\lambda} \right\} \right|^2 \\ &= I_0^2 \left| \int dx_0 t(x_0) \text{sinc} \left\{ \left( x_0 + \frac{x_t}{M_t} \right) \frac{L_t}{\lambda d_1} \right\} \text{sinc} \left\{ \left( x_0 + \frac{x_r}{M_r} \right) \frac{L_r}{\lambda d_3} \right\} \right|^2, \end{aligned} \quad (13)$$

where  $M_t = d_2/d_1$  and  $M_r = d_4/d_3$  are the magnifications of the imaging systems in the test arm and the reference arm, respectively. For a simple case of  $x_r = M_r x_t / M_t$ , Eq.(13) becomes

$$G \left( x_r = \frac{M_r}{M_t} x_t \right) \propto \left| \int dx_0 t(x_0) \text{sinc} \left\{ \left( x_0 + \frac{x_t}{M_t} \right) \frac{L_t}{\lambda d_1} \right\} \text{sinc} \left\{ \left( x_0 + \frac{x_t}{M_t} \right) \frac{L_r}{\lambda d_3} \right\} \right|^2 \quad (14)$$

which represents a special point-to-point intensity correlation and has the form of a coherent imaging scheme. Its kernel

$$h_g \left( x_r = \frac{M_r}{M_t} x_t \right) = \text{sinc} \left\{ \left( x_0 + \frac{x_t}{M_t} \right) \frac{L_t}{\lambda d_1} \right\} \text{sinc} \left\{ \left( x_0 + \frac{x_t}{M_t} \right) \frac{L_r}{\lambda d_3} \right\} \quad (15)$$

is the product of the 1-D APSFs of the two lenses, and analogous to the APSF of confocal laser scanning microscopy (CLSM) [1]. As shown in Fig.3, under the two lenses with same aperture  $L_r = L_t$ , the ratio between the full width at half maximum (FWHM) of  $h_g(x)$  (solid line B) and that of  $h_2(x_0, x_t)$  (dashed line A) is nearly 1/1.4, which suggests decreasing the spatial extent of the diffraction spot and increasing resolution by a factor of 1.4. What's more, the FWHM of  $h_g(x)$  can be further diminished by enlarging the aperture  $L_r$  of the lens in the reference arm (dotted line C), which is important to increase resolution of the two-arm imaging system with a low-NA lens in test arm.

In the experiment, the thermal source was simulated by the pseudo-thermal light generated by a frequency-doubled pulsed Nd:Yag laser ( $\lambda = 0.532 \mu\text{m}$ ) hitting a slowly rotating ground-glass disk, and two CCD cameras were used to record the light intensities of both arms, respectively. We first put a double slit (the slit width  $90 \mu\text{m}$  and the center-to-center separation  $180 \mu\text{m}$ ) in the object plane, and chose two lenses with same focal length ( $f_t = f_r = 400 \text{ mm}$ ) in the two arms. The transmission aperture  $L_t$  of the lens of the test arm was fixed at  $3 \text{ mm}$  by an iris diaphragm in the whole experimental process, while the aperture  $L_r$  in the reference arm could range from  $3$  to  $20 \text{ mm}$  by another iris diaphragm. Taking  $d_1 = d_2 = 2f_t$  and  $d_3 = d_4 = 2f_r$  made the magnification  $M_t = M_r = 1$ . As a result of Eq.(3), the resolution limit of the test arm is  $1.22\lambda d_1/L_t \approx 173 \mu\text{m}$ , approximately to the double-slit distance  $180 \mu\text{m}$ . Thus, we only distinguished the double slit barely by the imaging system of

the test arm and got a blurry image [see Fig.4(a)]. However, under the same aperture  $L_r = L_t = 3 \text{ mm}$ , we could gain a relatively clear image via the correlation between the two arms [Fig.4(b)]. Furthermore, a higher-resolution image was obtained by expanding  $L_r$  to  $6 \text{ mm}$  [Fig.4(c)]. Besides, keeping  $L_r = 3 \text{ mm}$  and  $M_r = 1$  invariant, we also got a better image by employing a lens with short focal length ( $f_r = 250 \text{ mm}$ ) in the reference arm [Fig.4(d)].

The quantitative comparison can be seen from the nor-

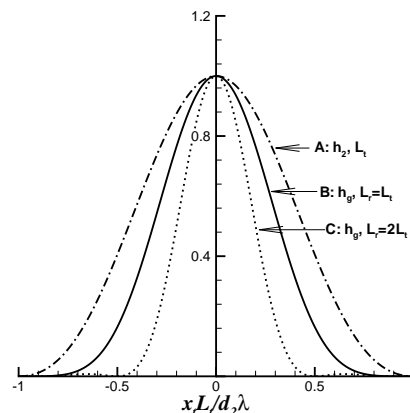


FIG. 3: The comparison between the FWHMs of  $h_2(x_0, x_t)$  and  $h_g(x)$ . Dashed line A is the 1-D APSF  $h_2(x_0, x_t)$  of a single lens with aperture  $L_t$ ; solid line B represents the kernel  $h_g(x)$  of the two-arm system under  $L_r = L_t$  and Dotted line C under  $L_r = 2L_t$ .

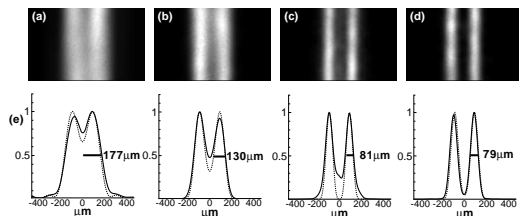


FIG. 4: The acquired images of the double slit from the two-arm imaging system. (a) was produced directly by the test arm under  $f_t = 400mm$ ,  $L_t = 3mm$ , and (b)-(d) were generated through the correlation between the same test arm and different reference arms under (b):  $f_r = 400mm$ ,  $L_r = 3mm$ ; (c):  $f_r = 400mm$ ,  $L_r = 6mm$ ; (d):  $f_r = 250mm$ ,  $L_r = 3mm$ . In (e), solid lines denote the normalized horizontal section of the images of (a)-(d), and dashed lines are corresponding theoretical curves.

malized horizontal section plotted in Fig.4(e) (solid line), which agrees with the theoretical analysis (dashed line). The images of a more complex object (a mask with letters “SIOM”) were gained by repeating above experimental processes [see Fig.5]. These results show that enhancing the resolving power of the reference arm where there is no object to be observed, can increase the resolution of the image effectively.

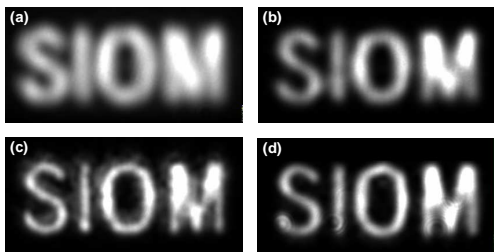


FIG. 5: The acquired images of the letters “SIOM” from the two-arm imaging system. The experimental parameters of (a)-(d) are the same with that of Fig.4(a)-(d), respectively.

It’s well known that medical endoscopes are very useful instruments in disease diagnosis. While the narrow space between human internal organs only allows the probe with a small lens into the body, which restricts the image resolution. To overcome the problem, a two-arm endoscope based on ghost imaging can be developed. Because of no test objects in the reference arm, the imaging system is not confined to the endoscopic working environment and may use a larger lens on the outside of the body to generate higher-resolution images through the correlation. And for transmission x-ray microscopes, the transverse resolution is equal to  $\beta\lambda/NA_F$ , where  $NA_F$  is the numerical aperture of a Fresnel zone plate and  $\beta$  is an illumination dependent constant [7]. The focal depth of the zone plate is calculated by  $\Delta z \approx \pm \frac{1}{2}\lambda/NA_F^2$ , following the definition of Born and Wolf [22]. Hence, as one increases  $NA_F$ , the resolution improves linearly, while the focal depth decreases as the square that limits the thickness of specimens under investigation. This dilemma can also be solved by a x-ray microscope with two arms: in the test arm using a Fresnel zone plate with long focal depth permits a certain penetration depth, and in the reference arm selecting another Fresnel zone plate of high NA guarantees required resolution. The two-arm imaging scheme is also applicable to many other microscopic systems where the NAs of their objective lenses are limited.

In conclusion, we have demonstrated the feasibility of a microscope scheme based on ghost imaging technique for improving the resolution of a lens-limited imaging system, and briefly discuss potential applications of this “ghost” microscope. Compared with CLSM, the two-arm microscope system has a similar APSF and also realizes high resolution, but is more flexible and convenient in manoeuvring optical components because its test arms and reference arm are two independent imaging systems.

This research is partially supported by the Hi-Tech Research and Development Program of China, Project No. 2006AA12Z115, and Shanghai Fundamental Research Project, Project No. 06JC14069.

- 
- [1] C.J.R. Sheppard and A. Choudhury, *Opt. Acta.* **24**, 1051-1073 (1977).  
[2] K. Carlsson, et al., *Opt. Lett.* **10**, 53-55 (1985).  
[3] B. Niemann, et al., *Appl. Opt.* **15**, 1883-1884 (1976).  
[4] G. Schmahl, et al., *Optik* **97**, 181-182 (1994).  
[5] E. Abbe, *Arch. f. Mikr. Anat.* **9**, 413-468 (1873).  
[6] R.M. Satava, et al., *Am. Surg.* **54**, 73-77 (1988).  
[7] C. Jacobsen, et al., *Ultramicroscopy* **47**, 55-79 (1992).  
[8] T.B. Pittman, et al., *Phys. Rev. A* **52**, R3429 (1995).  
[9] R.S. Bennink, et al., *Phys. Rev. Lett.* **89**, 113601 (2002).  
[10] Jing Cheng and Shensheng Han, *Phys. Rev. Lett.* **92**, 093903 (2004).  
[11] M. Bache et al., *Opt. Express* **12**, 6067 (2004).  
[12] A. Valencia, et al., *Phys. Rev. Lett.* **94**, 063601 (2005).  
[13] Da Zhang, et al., *Opt. Lett.* **30**, 2354 (2005).  
[14] Jin Cheng and Shensheng Han, *Phys. Rev. A* **76**, 023824 (2007).  
[15] A. Gatti, et al., *J. Mod. Opt.* **53**, 739 (2006).  
[16] Honglin Liu, et al., *Phys. Rev. A* **76**, 053808 (2007).  
[17] Yangjian Cai and Shi-Yao Zhu, *Phys. Rev. E* **71**, 056607 (2005).  
[18] M. D’Angelo, et al., *Phys. Rev. A* **72**, 013810 (2005).  
[19] Minghui Zhang, et al., *Phys. Lett. A* **366**, 569-574 (2007).  
[20] R.J. Glauber, *Phys. Rev.* **130**, 2529 (1963); R.J. Glauber, *Phys. Rev.* **131**, 2766 (1963).  
[21] L. Rayleigh, *Philos. Mag.* **8**, 261-274 (1879).  
[22] M. Born and E. Wolf, *Principles of Optics*, 7th ed., (Cambridge University Press, Cambridge, 1999), p.491.